Self-organized vascular networks from human pluripotent stem cells in a synthetic matrix

Sravanti Kusuma[a,b], Yu-I Shen[a], Donny Hanjaya-Putra[a], Prashant Mali[b,c,1], Linzhao Cheng[c], and Sharon Gerecht[a,d,2]

[a]Department of Chemical and Biomolecular Engineering, Johns Hopkins Physical Sciences–Oncology Center and Institute for NanoBioTechnology, and [b]Department of Biomedical Engineering, Johns Hopkins University, Baltimore, MD 21218; [c]Institute for Cell Engineering and Division of Hematology, Johns Hopkins School of Medicine, Baltimore, MD 21287; and [d]Department of Materials Science and Engineering, Johns Hopkins University, Baltimore, MD 21218

Edited by Robert Langer, Massachusetts Institute of Technology, Cambridge, MA, and approved June 14, 2013 (received for review April 7, 2013)

The success of tissue regenerative therapies is contingent on functional and multicellular vasculature within the redeveloping tissue. Although endothelial cells (ECs), which compose the vasculature's inner lining, are intrinsically able to form nascent networks, these structures regress without the recruitment of pericytes, supporting cells that surround microvessel endothelium. Reconstruction of typical in vivo microvascular architecture traditionally has been done using distinct cell sources of ECs and pericytes within naturally occurring matrices; however, the limited sources of clinically relevant human cells and the inherent chemical and physical properties of natural materials hamper the translational potential of these approaches. Here we derived a bicellular vascular population from human pluripotent stem cells (hPSCs) that undergoes morphogenesis and assembly in a synthetic matrix. We found that hPSCs can be induced to codifferentiate into early vascular cells (EVCs) in a clinically relevant strategy amenable to multiple hPSC lines. These EVCs can mature into ECs and pericytes, and can self-organize to form microvascular networks in an engineered matrix. These engineered human vascular networks survive implantation, integrate with the host vasculature, and establish blood flow. This integrated approach, in which a derived bicellular population is exploited for its intrinsic self-assembly capability to create microvasculature in a deliverable matrix, has vast ramifications for vascular construction and regenerative medicine.

codifferentiation | hydrogels

Perhaps the greatest roadblock to the success of tissue regenerative therapies is the establishment of a functional microvascular network to support tissue survival and growth (1). Microvascular construction or regeneration depends on endothelial morphogenesis into a 3D tubular network, followed by stabilization of the assembling structures by recruited pericytes (2, 3). To create such a construct for therapeutic applications, patient-derived ECs and pericytes must be incorporated into a synthetic matrix, which confers an advantage in controlling and modulating vascular morphogenesis and also represents a clinically relevant construct in which to deliver the engineered microvascular networks to in vivo environments (4).

Human pluripotent stem cells (hPSCs), including human embryonic stem cells (hESCs) and human induced PSCs (hiPSCs), offer the opportunity to derive EVCs from the same source, which offers patient specificity. Various cell markers have been proposed to identify vascular precursors (of ECs and pericytes) from differentiating hPSCs including CD34 (5, 6), VEGF receptor-2 (VEGFR2)/kinase domain receptor (KDR) (7), and apelin receptor (8). Purification of such progenitors is required from an uncontrolled differentiated cell population [i.e., via embryoid body (EB) formation or coculture on mouse feeder layer] through marker enrichment or selection through genetic manipulation. Importantly, none of these derived cells have been demonstrated to self-assemble into functional microvasculature containing both ECs and pericytes.

Current approaches for the differentiation of hPSCs toward the vascular lineage typically use a purified, single derivative—either a progenitor or a mature cell type—with the goal of fully characterizing the fidelity of differentiation from a PSC. From this body of work, it has become apparent that various cell markers and biochemical cues can be used to guide differentiation and derive functional ECs (5, 9–12), vascular smooth muscle cells (5, 11, 13) and pericytes (14). Building on these previous studies, in the present study we hypothesized that hPSCs can be induced to differentiate into early derivatives of the vascular lineage (i.e., EVCs) that compose the microvascular architecture without a specific differentiation-inducible feeder layer, EB formation, or genetic manipulation (Fig. 1*A*, *i*); and that such EVCs can mature into ECs and pericytes and can self-assemble to form vascular networks in an engineered matrix (Fig. 1*A*, *ii*).

We present a unique conceptual approach in which the cells of the microvasculature are derived in a bipotent population, which is able to recreate the tissue. Our protocol uses a monolayer culture and avoids an EB intermediate and sorting, thereby enabling reproducibility and clinical applicability. We harness intrinsic tissue-level differentiation and self-assembly capabilities toward the translational realization of hPSCs. This paradigm could prove useful for the construction of other multicellular tissues for regeneration.

Results and Discussion

Derivation of EVCs from hPSCs. Toward clinically relevant outcomes, and because microvascular architecture is a bicellular entity, we first sought to develop a robust and controlled method to differentiate hPSCs into a bicellular vasculogenic population with maturation capacity to both ECs and pericytes. CD105 and CD146 are common to both cell types (14–17), whereas vascular endothelial cadherin (VEcad) has been shown to specify a lineage commitment of ECs (10). Although no single marker designates pericytes, pericytes can be distinguished by the expression of platelet-derived growth factor β (PDGFRβ) in conjunction with CD146 (18).

Acknowledging that cocultures of pericytes and ECs typically result in pericyte-mediated EC growth inhibition (14, 19), we focused on inducing $VEcad^+$ cells early in the differentiation process to ensure EC maturation. Building on previous work (10, 20, 21), we developed a stepwise differentiation procedure to induce vascular lineage specification. hPSCs (*SI Appendix*, Table S1) were first allowed to undergo differentiation in a monolayer (*SI Appendix*, Fig. S1). The subsequent addition of TGF-β inhibitor SB431542 (10), supplemented with either high (50 ng/mL) or low (1 ng/mL) concentrations of VEGF-A yielded up-

Author contributions: S.K. and S.G. designed research; S.K., Y.-I.S., and D.H.-P. performed research; Y.-I.S., D.H.-P., P.M., and L.C. contributed new reagents/analytic tools; S.K., Y.-I.S., D.H.-P., and S.G. analyzed data; and S.K., L.C., and S.G. wrote the paper.

The authors declare no conflict of interest.

This article is a PNAS Direct Submission.

[1]Present address: Department of Genetics, Harvard Medical School, Boston, MA 02115.

[2]To whom correspondence should be addressed. E-mail: gerecht@jhu.edu.

This article contains supporting information online at www.pnas.org/lookup/suppl/doi:10.1073/pnas.1306562110/-/DCSupplemental.

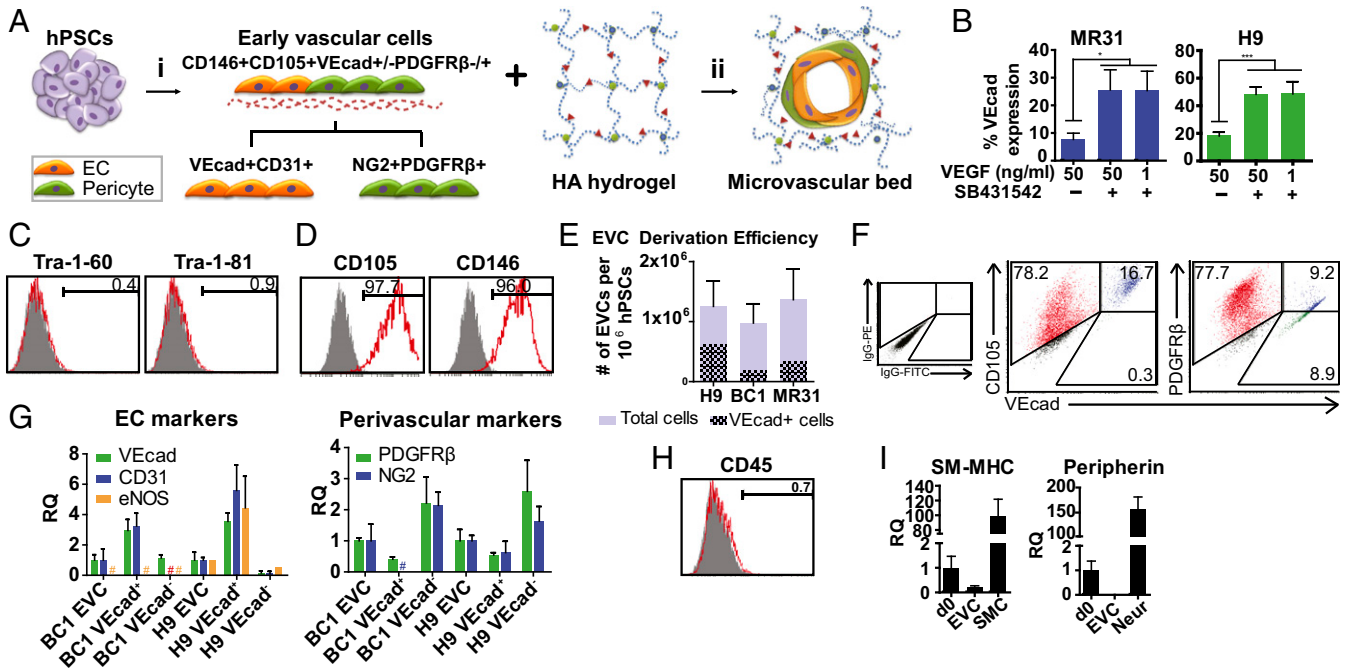

Fig. 1. Derivation of EVCs from hPSCs. (*A*) Schema for self-assembled vascular derivatives. (*i*) hPSCs are differentiated toward EVCs that can be matured into functional ECs and pericytes. (*ii*) Derived EVCs are embedded within a synthetic HA matrix that facilitates self-organization into vascular networks. (*B*) VEcad expression in day 12 differentiated hiPSC-MR31 and hESC-H9 cell lines comparing the three differentiation conditions tested (flow cytometry analysis; $n = 3$). (*C* and *D*) Flow cytometry plots ($n = 3$) of EVC derivatives assessing the expression of pluripotent markers TRA-1-60 and TRA-1-81 (*C*) and CD105 and CD146 (*D*). (*E*) EVC differentiation efficiency from hPSC lines per 1 million input hPSCs. (*F*) Flow cytometry plots ($n = 3$) of EVC derivatives assessing expression of VEcad double-labeled with CD105 or PDGFRβ. (*Left*) Isotype controls. (*G*) Quantitative RT-PCR analysis of EC and perivascular marker expression by EVCs and sorted VEcad$^+$ and VEcad$^-$ cells. # denotes not detected. Data are normalized to EVCs of each specific hPSC type. (*H*) Flow cytometry plots ($n = 3$) of hematopoietic marker CD45 (hiPSC-BC1). (*I*) Quantitative RT-PCR of H9-EVCs for the expression of SMMHC and peripherin, compared with undifferentiated cells (d0) and mature derivatives (13, 37). Isotype controls for flow cytometry are in gray. Flow cytometry results shown are typical of the independent experiments. $^*P < 0.05$; $^{**}P < 0.01$; $^{***}P < 0.001$.

regulation of VEcad expression ranging from 20% to 60% VEcad$^+$ cells, depending on hPSC line (Fig. 1*B* and *SI Appendix*, Fig. S2).

Under our differentiation strategy, hESC line H9 exhibited the greatest potential to yield the largest percentage of VEcad$^+$ cells compared with hiPSC lines BC1 and MR31. The expression levels of CD31 were not changed under the various conditions, whereas VEGFR2/KDR expression was higher in media supplemented with a low VEGF concentration (*SI Appendix*, Fig. S3). Expression of tumor rejection antigen (TRA)-1-60 and TRA-1-81, markers of pluripotency, was <1% when using high VEGF concentrations, indicating that the vast majority of cells had been differentiated (Fig. 1*C* and *SI Appendix*, Fig. S3). Thus, in all experiments, EVCs were differentiated in medium supplemented with SB431542 and with high VEGF concentrations.

EVCs derived from multiple hPSC lines using high VEGF concentrations and SB431542 were highly purified (>95%) for CD105 and CD146, surface antigens common to both ECs and pericytes (Fig. 1*D* and *SI Appendix*, Fig. S4 *A–C*), expanding on a previously reported approach that sorted out a CD105$^+$ population from spontaneously differentiating EBs with the focus on pericytes (14). By eliminating a sorting step and guiding hPSCs toward a bipotent population, our approach builds on this previous study and provides a unique strategy to yield a CD105$^+$ CD146$^+$ population that composes the bicellular microvascular architecture in a controlled, efficient, and robust manner.

Without our specific inductive protocol (i.e., removal of VEGF and SB431542 supplementation), hiPSC-BC1 cells differentiated for 12 d were still fairly well enriched in CD105 (95%) and CD146 (93%); however, hESC-H9 cells differentiated for 12 d without these inductive conditions expressed ~90% CD105$^+$ cells and only 54% CD146$^+$ cells (*SI Appendix*, Fig. S4*D*). Importantly, both H9 and BC1 differentiated cell populations expressed very low levels of VEcad. These results, along with the aforementioned finding that high VEGF supplementation ensures <1% TRA-1-60$^+$ cells in the various hPSC types (Fig. 1*C* and *SI Appendix*, Fig. S3), further support our choice of inductive media conditions.

Using our approach, we derived CD105$^+$CD146$^+$ EVCs at an approximate ratio of 1:1 of input hPSC to EVC (Fig. 1*E*). The number of input hPSCs was calculated as the number seeded at day 0, not the number of cells present after 1 d of differentiation, as reported previously (10). The yield of VEcad$^+$ cells in EVCs varied among cell lines, ranging from ~8×10^4 to 2.5×10^5 per 10^6 hPSCs (Fig. 1*E*), similar to what has been recently reported for KDR$^+$ EC derivatives (22). Flow cytometry analysis of EVCs double-labeled with antibodies against CD105 and VEcad confirmed that a subset of cells coexpressed CD105 and VEcad (Fig. 1*F*, *Left*). In contrast, EVCs double-labeled for VEcad and PDGFRβ revealed two distinct VEcad$^+$PDGFRβ^{lo} and VEcad$^-$PDGFRβ$^+$ populations (Fig. 1*F*, *Right* and *SI Appendix*, Fig. S5).

RT-PCR analysis of sorted VEcad$^+$ and VEcad$^-$ subpopulations from EVCs revealed distinct phenotypes (Fig. 1*G*). VEcad$^+$ cells from both hESC-H9 and hiPSC-BC1 cell lines demonstrated greater expression of EC markers VEcad and CD31 compared with unsorted EVCs and sorted VEcad$^-$ subpopulations. Of note, endothelial nitric oxide synthase (eNOS), a mature EC marker, was highly expressed in H9-VEcad$^+$ cells compared with H9 EVCs and sorted VEcad$^-$ cells, whereas

eNOS was undetected in all tested BC1 samples. Sorted VEcad$^-$ cells exhibited greater expression of pericyte markers PDGFRβ and NG2 compared with EVCs and sorted VEcad$^+$ cells.

Our analysis also revealed differences in the differentiation potential between hESC-H9 and hiPSC-BC1 lines using the adherent, stepwise differentiation protocol, suggesting that hESC-H9–differentiating cells may mature more rapidly toward these lineages, owing to the fact that 12-d differentiated H9-EVCs started to express eNOS at the mRNA level and yielded a greater percentage of VEcad$^+$ (Fig. 1*B*) and CD31$^+$ cells at the protein level (*SI Appendix*, Fig. S3) compared with the tested hiPSC lines.

EVCs were negative for hematopoietic marker CD45 (Fig. 1*H*), and demonstrated negligible expression of the smooth muscle cell marker smooth muscle myosin heavy chain (SMMHC), as well as the peripheral neuron marker peripherin (Fig. 1*I*). Comparable marker expression profiles were obtained from EVCs derived using serum-free conditions in our adherent differentiation scheme (*SI Appendix*, Fig. S6). Based on these analyses, we considered this derived population to be vascular lineage-specific and composed of early ECs and early pericytes. It should be noted that these are not mature ECs and pericytes, given that 12 d of differentiation was not sufficient to mature hPSCs toward matured phenotypes, in agreement with numerous previous studies (5, 14, 23).

Maturation of EVCs: ECs. We took two approaches to examine the endothelial potential of hPSC-EVCs, (*i*) subculturing EVCs and (*ii*) sorting and expanding VEcad$^+$ cells, both under the same culture conditions (i.e., 50 ng/mL VEGF and SB431542). Subculturing yielded ECs that were enriched in VEcad and CD31 (*SI Appendix*, Fig. S7 *A* and *B*); however, this approach and enrichment without cell sorting varied among three different hPSC lines, and a hiPSC line with vector integration demonstrated the best results (*SI Appendix*, Fig. S7*C*). Sorted VEcad$^+$ cells from EVCs matured toward VEcad$^+$CD31$^+$CD146$^+$ ECs (Fig. 2*A*). The cells exhibited typical membrane expression of VEcad and CD31, lectin binding, cytoplasmic expression of eNOS and von Willebrand factor (vWF), uptake of acetylated low-density lipoprotein (acLDL), up-regulation of intercellular adhesion molecule 1 (ICAM1) in response to TNF-α, and network formation on Matrigel (Fig. 2*B* and *SI Appendix*, Fig. S7 *D* and *E*). We did not detect lectin, eNOS, vWF, or acLDL uptake via immunofluorescence in our unsorted EVC populations, demonstrating that no subpopulation of EVCs expresses these EC characteristics and that additional culture is needed to mature early ECs from EVCs. These findings were consistent among the different hPSC lines examined.

Maturation of EVCs: Pericytes. We next probed the pericyte potential of the EVCs. EVCs, which do not express NG2 (*SI Appendix*, Fig. S8*A*), were cultured under pericyte-inducing conditions (19). After 6 d of culture, cells were enriched in pericyte markers CD73, NG2, PDGFRβ, and CD44 (24) and depleted in EC markers VEcad and CD31 (Fig. 2*C* and *SI Appendix*, Fig. S8*A*). Interestingly, most cells retained CD146$^+$ expression, but some lost CD105 expression (Fig. 2*C*). The spindle-shaped pericyte derivatives expressed PDGFRβ and NG2 proteoglycan and exhibited filamentous calponin expression (Fig. 2*D*), as would be expected for pericytes derived from fetal and adult sources. Sorted VEcad$^+$ cells were not able to attach and grow under pericyte-maturing conditions. An important function of pericytes is their ability to behave as mesenchymal precursors (14, 18). Indeed, the pericyte derivatives in our culture could be differentiated to adipocytes and osteoblasts (*SI Appendix*, Fig. S8 *B* and *C*), demonstrating their mesenchymal potential.

Furthermore, sorted VEcad$^-$ cells, cultured under either EC maturation conditions (50 ng/mL VEGF and SB431542) or pericyte-maturing conditions for 6 d, expressed NG2, PDGFRβ, and CD44 (*SI Appendix*, Fig. S9). A small population (~8%) of sorted VEcad$^-$ cells acquired VEcad expression (but not CD31 expression) when cultured under EC maturation conditions, indicating some degree of cellular plasticity.

Taken together, our cellular analysis results demonstrate that EVCs composed of CD105$^+$CD146$^+$VEcad$^+$ and CD105$^+$CD146$^+$PDGFRβ$^+$ subtypes contain the cellular makeup necessary for constructing a microvasculature.

Self-Organization of Bicellular Vascular Networks in Hydrogels. To examine whether EVCs could be leveraged to self-organize into a bicellular microvascular bed, we tested network formation in collagen (2, 25) and in completely synthetic hyaluronic acid (HA)-based hydrogel (3) (Fig. 3*A* and *SI Appendix*, Fig. S10). We speculated that derived EVCs would be able to form vascular networks in a 3D matrix. Indeed, in both hydrogel systems, EVCs were found to form lavish networks (Fig. 3*A*); sorted VEcad$^+$ or VEcad$^-$ cells individually were unable to form such networks when encapsulated within collagen gels (Fig. 3*B*). VEcad$^+$ cells

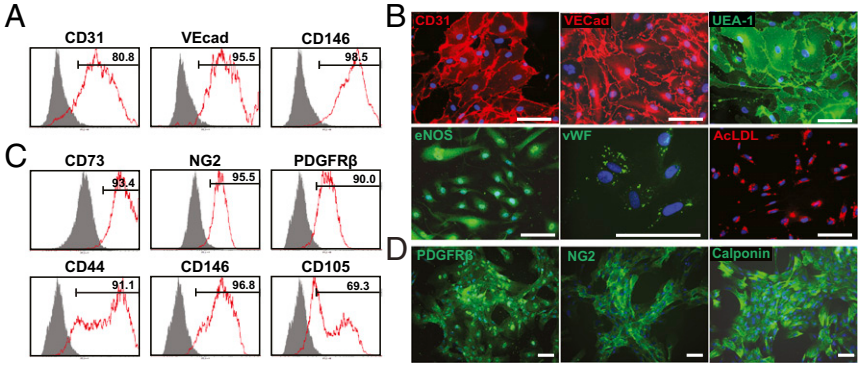

Fig. 2. EVC maturation. (*A*) Sorted VEcad$^+$ from hiPSC-BC1–derived EVCs subcultured for an additional 6 d in 50 ng/mL VEGF and SB431542-supplemented conditions and analyzed for the expression of VEcad, CD31, and CD146 (representative flow cytometry plots; $n = 3$). (*B*) Subcultured sorted VEcad$^+$ from hiPSC-BC1–derived EVCs exhibited membrane localization of CD31 and VEcad (both in red), lectin binding (in green), cytoplasmic expression of eNOS, punctuated vWF, and uptake of acLDL (in red). (*C*) hiPSC-BC1–derived EVCs subcultured for an additional 6 d in pericyte-inducing conditions (19) were analyzed for the expression of NG2, CD73, PDFGRβ, CD44, CD146, and CD105 via flow cytometry. (*D*) Immunofluorescence analysis revealed appropriate localization of PDGFRβ, NG2, and calponin (all in green). Isotype controls for flow cytometry are in gray, and nuclei are in blue. Results shown are typical of the independent experiments. (Scale bars: 100 μm.)

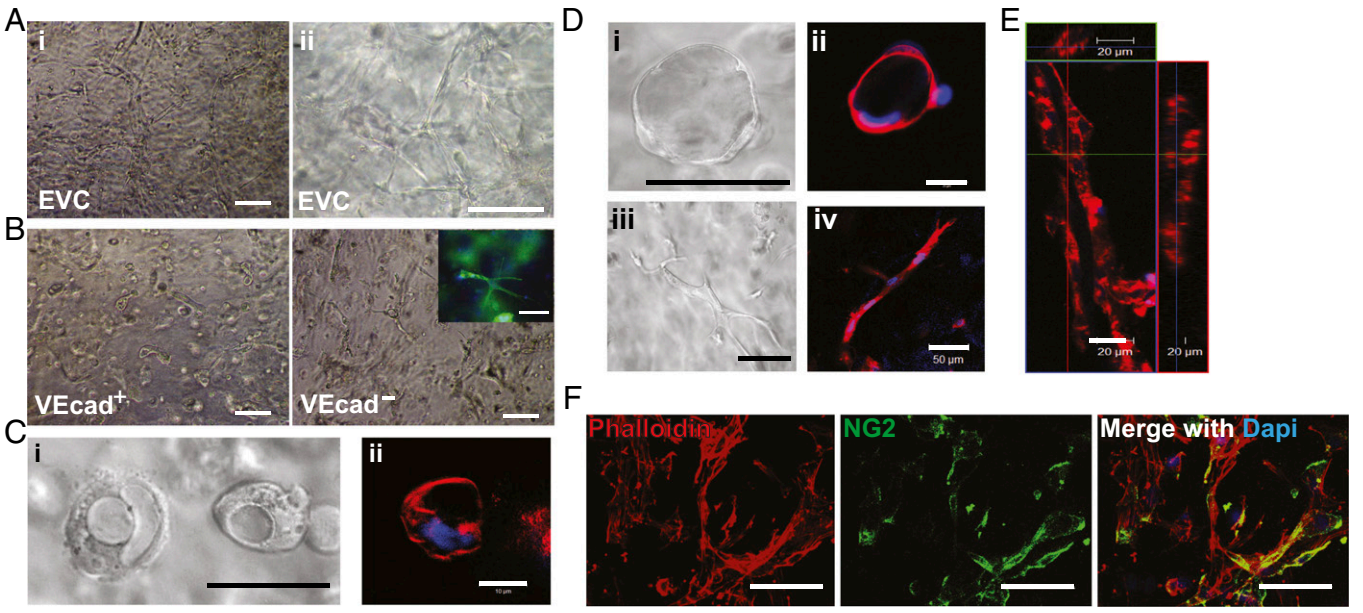

Fig. 3. Self-assembly of EVCs to multicellular networks in a 3D matrix. (*A*) Network formation from BC1-EVCs in collagen (*i*) and HA hydrogels (*ii*). (*B*) Sorted VEcad$^+$ and VEcad$^-$ cells encapsulated within collagen gels were unable to form networks. (*Insert*) Example of a cell with typical stellate morphology, with phalloidin in green and nuclei in blue. (Scale bars: 100 μm.) (*C*) Vacuole formation was observed after one day as evidenced by light microscopy (LM) (i) and confocal images (*ii*) of vacuole vital stain, FM4-64, in red and nuclei in blue. (Scale bar: 10 μm.) (*D*) On day 2, network formation with enlarged lumen (*i* and *ii*) and cell sprouting (*iii* and *iv*) were visualized by LM images (*i* and *iii*) and confocal images (*ii* and *iv*) of FM4-64 in red and nuclei in blue. (Scale bars: 10 μm in *i* and *iii*; 20 μm in *ii*; 50 μm in *iv*.) (*E*) On day 3, complex networks were observed with enlarged and open lumen, as indicated by confocal z-stacks and orthogonal sections of FM4-64 in red and nuclei in blue. (Scale bar: 20 μm.) (*F*) After 3 d, multilayered structures were also detected, as demonstrated by a 3D projection image of NG2 (green), phalloidin (red), and nuclei (blue) showing NG2$^+$ pericytes integrated onto hollow structures. Images shown are typical of the independent experiment. (Scale bars: 50 μm.)

formed primarily vacuoles and started to form nascent structures within the collagen gel, with some instances of sprouting (Fig. 3*B*).

We attribute the lack of robust network formation from derived ECs in collagen gels to the lack of pericytes in culture, and speculate that the addition of support cells help form the networks seen with EVC encapsulation. VEcad$^-$ cells exhibited cell spreading and a characteristic stellate morphology, but no network formation (Fig. 3*B*).

Vascular Morphogenesis of EVCs Within HA Hydrogels. We next examined the progress of EVC network formation within the HA hydrogel, a xeno-free synthetic construct engineered to recapitulate tubulogenesis-inducing signals (3). In vitro assessment of cellular behavior revealed the formation of multicellular networks via a sequential process typical of vascular morphogenesis. After 1 d of culture, we observed vacuole formation in many, but not all, of the cells. Some of these vacuoles had coalesced into a larger structure, resembling lumen (Fig. 3*C* and *SI Appendix*, Fig. S11*A*).

To elucidate the phenotype of either cell type after 1 d, we also encapsulated VEcad$^+$ and VEcad$^-$ subpopulations independently. After 1 d, we clearly observed vacuoles in the encapsulated sorted VEcad$^+$ subpopulation after 1 d; however, encapsulated sorted VEcad$^-$ cells primarily spread, with no vacuole formation (*SI Appendix*, Fig. S11 *B* and *C*).

After 2 d of EVC encapsulation, we observed the progression of tubulogenesis, including extensive sprouting and an occasional open lumen (Fig. 3*D* and *SI Appendix*, Fig. S12*A*). By day 3, vascular networks had grown, with comprehensive multicellular networks clearly visible within HA hydrogels. Complex vascular networks with patent lumen structures were readily detected throughout the hydrogels, suggesting an engineered vascular network (Fig. 3*E* and *SI Appendix*, Fig. S12*B*). Interestingly, on day 3, we detected NG2$^+$ pericytes incorporated in the luminal structures and encircling the emerging tubular structures (Fig. 3*F* and *SI Appendix*, Fig. S13).

Integration of hPSC-Bicellular Microvascular Constructs. In vivo integration of vascular networks is crucial to the success of derived EVCs in regenerative medicine applications. We first tested whether EVCs can survive implantation, assemble into microvascular networks, integrate with the host vasculature, and establish blood flow. A Matrigel plug assay (5) revealed EVCs incorporated with perfused host microvasculature and generated human-only microvascular structures (*SI Appendix*, Fig. S14).

Next, to harness the self-organizing capability of EVCs in HA hydrogels, we implanted the engineered microvascular networks s.c. and assessed their survival and integration after 2 wk. We found that EVCs (derived from a BC1 or GFP-hiPSC cell line) were incorporated into or wrapped around the mouse microvasculature (Fig. 4 *A* and *B* and *SI Appendix*, Fig. S15), and that the hydrogels were largely degraded by 2 wk. HA gels without encapsulated cells exhibited slower remodeling and degradation in vivo compared to gels with cells, as we reported previously (3). Perfused microvasculature (as indicated by tail-injected, mouse-specific fluorescein-conjugated *GS-IB4* lectin) containing human ECs (with cross-sectional areas ranging from 100 to 25,000 μm^2) were abundant throughout the explant (~15 vessels per mm^2), demonstrating that the transplanted human vascular networks had anastomosed with the host circulatory systems (Fig. 4 *C*–*E*). Moreover, NG2$^+$ human pericytes were found to migrate toward and encircle the perfused vasculature (Fig. 4*F* and *SI Appendix*, Fig. S16).

Although our bicellular constructs present several fundamental advancements to the future of cell-based therapies, additional studies are needed to fine-tune the ratio of early ECs to pericytes within EVC populations, owing to the wide variability of this

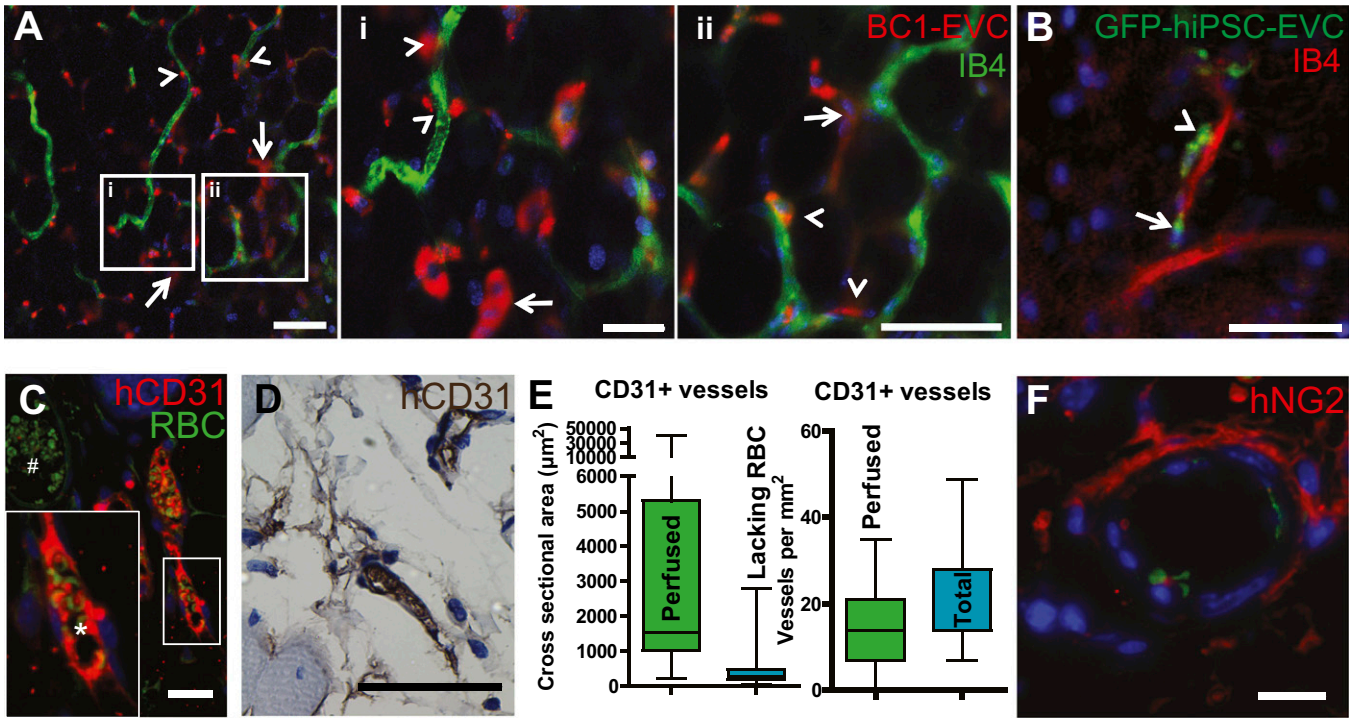

Fig. 4. Perfusion of EVC networks in vivo in synthetic hydrogels. (*A* and *B*) Confocal images of 2-wk explants of BC1-EVC (*A*) or GFP-hiPSC-EVC (*B*) networks in HA hydrogels demonstrate incorporation of human cells (*A*, red; *B*, green; arrows) into host vessels (tail vein-injected, mouse-specific Alexa Fluor 488-conjugated (*A*) or Alexa Fluor 546-conjugated (*B*) *GS-IB4* lectin and human cells exhibiting pericyte behavior (arrowheads). (Scale bars: 50 μm.) (*i* and *ii*) High-magnification views of indicated regions. (*C* and *D*) Histological examination of the explants stained for human specific CD31 expression via immunofluorescence (CD31 in red; RBCs in green; DAPI in blue) (*C*) and immunohistochemistry (CD31 in brown, counterstain in blue) reveals functional vessels containing human CD31$^+$ cells with perfused blood cells (*D*). *Perfused human vessel; #perfused mouse vessel. (Scale bars: 10 μm in *C*; 50 μm in *D*.) (*E*) Quantification of cross-sectional areas and vessels per mm^2 of microvasculature containing human CD31$^+$ cells depicts large perfused vessels and smaller vessels lacking RBCs in explants. (*F*) Immunofluorescence staining of sectioned explants for human specific NG2$^+$ (red) cells reveals functional human pericytes wrapping perfused vessels. RBCs are in green, and DAPI is in blue. (Scale bar: 10 μm.)

ratio in different tissues and organs (26). Further investigation is also needed for clinical translation, including understanding of cell–cell interactions and appreciation of the longevity and durability of the human vascular networks. Future studies should focus on determining the in vivo longevity of engineered human networks to reveal not only the long-term integration of the human vasculature in the tissue, but also whether teratoma formation is of concern, a vital consideration of pluripotent stem cell therapies.

The balance between commitment and plasticity of the EVCs specifically within the vascular lineage allows for vascular fate and network maturation. This controlled system is reproducible, generates physiologically relevant vascular networks in implantable matrices, and thus provides the next fundamental step toward patient-specific engineered tissue with clinically translatable potential.

Experimental Procedures

Detailed descriptions of the materials and methods used in this study are provided in *SI Appendix, Materials and Methods*.

hPSC Culture. The hESC lines H9 and H13 (passages 15–40; WiCell Research Institute) and hiPSC lines MR31 (27), MMW2 (28), BC1 (29, 30), and a GFP transgenic hiPSC line (clone 26 hCBiPS aMHCneoPGKhygro + pCAGGS2 passage 47+10, kindly provided by Dr. Ulrich Martin, Hannover Medical School, Hannover, Germany) (31) were cultured as described previously (13, 32). Cell lines were routinely examined for pluripotent markers using immunofluorescence staining and flow cytometry analysis for TRA-1-60, TRA-1-81, stage-specific embryonic antigen-4 (SSEA4), and Oct4. Details of the various hPSCs are provided in *SI Appendix*, Table S1.

Differentiation Protocol. hPSCs were collected through digestion with EDTA (Promega), separated into an individual cell suspension using a 40-μm mesh strainer (BD Biosciences), and plated onto collagen IV (Trevigen)-coated plates at a concentration of 5×10^4 cells/cm^2. Cells were cultured for 6 d in a differentiation medium composed of alpha-MEM (Invitrogen), 10% FBS (HyClone), and 0.1 mM β-mercaptoethanol (β-ME), with the medium changed daily. On day 6, differentiated cells were collected through digestion with TrypLE (Invitrogen), separated with a 40-μm mesh strainer, and seeded at a concentration of 1.25×10^4 cells/cm^2 on collagen type IV-coated plates in endothelial cell growth media (ECGM) (PromoCell) supplemented with 2% FBS, 50 ng/mL VEGF with or without 10 μM SB431542 (Tocris), or 1 ng/mL VEGF plus 10 μM SB431542, for 6 d. The medium was changed every other day.

To elucidate whether serum-free conditions could be used to derive EVCs, we followed the aforementioned protocol, except differentiating the cells in alpha-MEM media supplemented with 20% knockout serum replacement, 0.1 mM β-ME, 1× nonessential amino acids (Gibco), and 1× L-glutamine (Invitrogen) for 6 d, followed by 6 d in ECGM base media (Promocell) supplemented with 50 ng/mL VEGF, 10 μM SB431542, 10% knockout serum replacement, β-ME, essential amino acids, and glutamine. These conditions were used only when specified in the text for serum-free differentiation.

EC Maturation. On day 12, derived EVCs were either subcultured in EC differentiation medium or sorted for VEcad$^+$ cells. For the latter, EVCs were collected through digestion with magnetic activated cell sorting (MACS) buffer (0.5 M EDTA and 1% BSA in PBS), incubated with 10 μL of anti-human PE-conjugated VEcad (BD Biosciences) in MACS buffer for 45 min on ice, washed, incubated again with 20 μL of anti-PE microbeads (Miltenyi Biotec) in 80 μL of MACS buffer for 15 min at 4 °C, and finally washed twice. Cells were resuspended in 500 μL of MACS buffer and separated using a MS MACS separation column (Miltenyi Biotec). VEcad enrichment or depletion was confirmed by flow cytometry. Sorted cells were cultured on collagen type

IV-coated dishes for an additional 6 d in ECGM supplemented with 50 ng/mL VEGF and 10 μM SB431542. The medium was changed every other day.

Pericyte Maturation. We followed a published protocol for pericyte maturation (19). On day 12, derived EVCs were collected through digestion with TrypLE and replated on tissue culture-treated six-well plates in medium composed of DMEM and 10% FBS. After 2–3 h, unattached cells were removed, and the medium was replaced. Cells were cultured for 6 d, with the medium changed every other day.

HA Gels. Acrylated HA hydrogels were prepared as reported previously (3, 33, 34). Derived EVCs or sorted subpopulations were encapsulated in HA hydrogels at a density of 4×10^6 cells/mL and cultured for up to 3 d in endothelial growth media 2 (EGM2; Lonza). Visualization and image acquisition were performed using an inverted light microscope (Olympus) and a confocal microscope (Zeiss LSM 510 Meta) along the culture. FM-464 vacuole staining (Invitrogen) was performed following the manufacturer's protocol (3). To test parallel differentiation, EVCs were also cultured in adherent culture in EGM2 for 3 d, with daily medium changes.

Implantation of Cells. Except for GFP-hiPSC–derived cells, all other PSCs (hiPSC-MR31, hESC-H9, hiPSC-BC1)-derived cells were labeled with PKH-26 (red) according to the manufacturer's protocol and as described previously (13). PKH-26–labeled cells were resuspended with Matrigel and 50 ng/mL bFGF or engineered vascular networks in HA gels for 3 d, then implanted s.c. into nude 6- to 8-wk-old female mice in quadruplicate. To visualize angiogenesis in the implants before sample removal after 2 wk, we injected Alexa Fluor 488 (or in some cases, Alexa Fluor 546 or 647)-conjugated isolectin GS-IB4 from *Griffonia simplicifolia* (Invitrogen) through the tail veins of the mice (35). After 20 min, mice were euthanized by CO_2 asphyxiation, after which the explants were harvested and fixed in 3.7% formaldehyde (Sigma-Aldrich) and proceeded for visualization and sectioning. The Johns Hopkins University's Institutional Animal Care and Use Committee approved all animal protocols.

Graphs and Statistics. All analyses were performed in triplicate samples for $n = 3$ at least. Quantitative RT-PCR was also performed on triplicate samples ($n = 3$) with triplicate readings. One-way ANOVA with the Bonferroni post hoc test were performed to determine significance using GraphPad Prism 4.02.

ACKNOWLEDGMENTS. We thank M. Wanjare for input on smooth muscle lineage differentiation; S. H. Tan, E. Peijnenburg, P. Patel, B. Macklin, and S. Zhao for technical assistance; S. Khetan and J. Burdick (University of Pennsylvania) for HA; Z. Binder for assistance with immunohistochemistry; Y. J. Kim and G. Lee for input on neuronal markers and providing the positive control; K. Schwanke and M. Ulrich (Hannover Medical School) for kindly providing GFP transgenic hiPSCs; and D. Hutton and W. L. Grayson for their expertise and assistance with adipogenic and osteogenic differentiations. This work was supported by predoctoral awards from the American Heart Association and National Institutes of Health (NIH) Grant F31HL112644 (both to S.K.), NIH Grant 2R01 HL073781 (to L.C.), NIH Grants R01 HL107938 and U54CA143868, an American Heart Association Scientist Development grant, and National Science Foundation Grant 1054415 (to S.G).

1. Discher DE, Mooney DJ, Zandstra PW (2009) Growth factors, matrices, and forces combine and control stem cells. *Science* 324(5935):1673–1677.
2. Stratman AN, Malotte KM, Mahan RD, Davis MJ, Davis GE (2009) Pericyte recruitment during vasculogenic tube assembly stimulates endothelial basement membrane matrix formation. *Blood* 114(24):5091–5101.
3. Hanjaya-Putra D, et al. (2011) Controlled activation of morphogenesis to generate a functional human microvasculature in a synthetic matrix. *Blood* 118(3):804–815.
4. Vunjak-Novakovic G, Scadden DT (2011) Biomimetic platforms for human stem cell research. *Cell Stem Cell* 8(3):252–261.
5. Ferreira LS, et al. (2007) Vascular progenitor cells isolated from human embryonic stem cells give rise to endothelial and smooth muscle-like cells and form vascular networks in vivo. *Circ Res* 101(3):286–294.
6. Park S-W, et al. (2010) Efficient differentiation of human pluripotent stem cells into functional $CD34^+$ progenitor cells by combined modulation of the MEK/ERK and BMP4 signaling pathways. *Blood* 116(25):5762–5772.
7. Yang L, et al. (2008) Human cardiovascular progenitor cells develop from a KDR^+ embryonic stem cell-derived population. *Nature* 453(7194):524–528.
8. Vodyanik MA, et al. (2010) A mesoderm-derived precursor for mesenchymal stem and endothelial cells. *Cell Stem Cell* 7(6):718–729.
9. Wang ZZ, et al. (2007) Endothelial cells derived from human embryonic stem cells form durable blood vessels in vivo. *Nat Biotechnol* 25(3):317–318.
10. James D, et al. (2010) Expansion and maintenance of human embryonic stem cell-derived endothelial cells by TGFbeta inhibition is Id1 dependent. *Nat Biotechnol* 28(2):161–166.
11. Drukker M, et al. (2012) Isolation of primitive endoderm, mesoderm, vascular endothelial and trophoblast progenitors from human pluripotent stem cells. *Nat Biotechnol* 30(6):531–542.
12. Rufaihah AJ, et al. (2013) Human induced pluripotent stem cell-derived endothelial cells exhibit functional heterogeneity. *Am J Transl Res* 5(1):21–35.
13. Wanjare M, Kuo F, Gerecht S (2013) Derivation and maturation of synthetic and contractile vascular smooth muscle cells from human pluripotent stem cells. *Cardiovasc Res* 97(2):321–330.
14. Dar A, et al. (2012) Multipotent vasculogenic pericytes from human pluripotent stem cells promote recovery of murine ischemic limb. *Circulation* 125(1):87–99.
15. Duff SE, Li C, Garland JM, Kumar S (2003) CD105 is important for angiogenesis: Evidence and potential applications. *FASEB J* 17(9):984–992.
16. Bardin N, et al. (2001) Identification of CD146 as a component of the endothelial junction involved in the control of cell-cell cohesion. *Blood* 98(13):3677–3684.
17. Airas L, et al. (1995) CD73 is involved in lymphocyte binding to the endothelium: Characterization of lymphocyte-vascular adhesion protein 2 identifies it as CD73. *J Exp Med* 182(5):1603–1608.
18. Crisan M, et al. (2008) A perivascular origin for mesenchymal stem cells in multiple human organs. *Cell Stem Cell* 3(3):301–313.
19. Orlidge A, D'Amore PA (1987) Inhibition of capillary endothelial cell growth by pericytes and smooth muscle cells. *J Cell Biol* 105(3):1455–1462.
20. Gerecht-Nir S, Ziskind A, Cohen S, Itskovitz-Eldor J (2003) Human embryonic stem cells as an in vitro model for human vascular development and the induction of vascular differentiation. *Lab Invest* 83(12):1811–1820.
21. Yamashita J, et al. (2000) Flk1-positive cells derived from embryonic stem cells serve as vascular progenitors. *Nature* 408(6808):92–96.
22. White MP, et al. (2013) Limited gene expression variation in human embryonic stem cell and induced pluripotent stem cell-derived endothelial cells. *Stem Cells* 31(1):92–103.
23. Wang L, et al. (2004) Endothelial and hematopoietic cell fate of human embryonic stem cells originates from primitive endothelium with hemangioblastic properties. *Immunity* 21(1):31–41.
24. Crisan M, Corselli M, Chen WC, Péault B (2012) Perivascular cells for regenerative medicine. *J Cell Mol Med* 16(12):2851–2860.
25. Stratman AN, et al. (2009) Endothelial cell lumen and vascular guidance tunnel formation requires MT1-MMP–dependent proteolysis in 3-dimensional collagen matrices. *Blood* 114(2):237–247.
26. Armulik A, Abramsson A, Betsholtz C (2005) Endothelial/pericyte interactions. *Circ Res* 97(6):512–523.
27. Mali P, et al. (2010) Butyrate greatly enhances derivation of human induced pluripotent stem cells by promoting epigenetic remodeling and the expression of pluripotency-associated genes. *Stem Cells* 28(4):713–720.
28. Zou J, Mali P, Huang X, Dowey SN, Cheng L (2011) Site-specific gene correction of a point mutation in human iPS cells derived from an adult patient with sickle cell disease. *Blood* 118(17):4599–4608.
29. Chou BK, et al. (2011) Efficient human iPS cell derivation by a non-integrating plasmid from blood cells with unique epigenetic and gene expression signatures. *Cell Res* 21(3):518–529.
30. Cheng L, et al.; NISC Comparative Sequencing Program (2012) Low incidence of DNA sequence variation in human induced pluripotent stem cells generated by non-integrating plasmid expression. *Cell Stem Cell* 10(3):337–344.
31. Haase A, et al. (2009) Generation of induced pluripotent stem cells from human cord blood. *Cell Stem Cell* 5(4):434–441.
32. Vo E, Hanjaya-Putra D, Zha Y, Kusuma S, Gerecht S (2010) Smooth-muscle-like cells derived from human embryonic stem cells support and augment cord-like structures in vitro. *Stem Cell Rev* 6(2):237–247.
33. Khetan S, Burdick JA (2010) Patterning network structure to spatially control cellular remodeling and stem cell fate within 3-dimensional hydrogels. *Biomaterials* 31(32):8228–8234.
34. Khetan S, Katz JS, Burdick JA (2009) Sequential crosslinking to control cellular spreading in 3-dimensional hydrogels. *Soft Matter* 5(8):1601–1606.
35. Kang K-T, Allen P, Bischoff J (2011) Bioengineered human vascular networks transplanted into secondary mice reconnect with the host vasculature and re-establish perfusion. *Blood* 118(25):6718–6721.
36. Lee G, Chambers SM, Tomishima MJ, Studer L (2010) Derivation of neural crest cells from human pluripotent stem cells. *Nat Protoc* 5(4):688–701.